



Real-time direct cell concentration and viability determination using a fully automated microfluidic platform for standalone process monitoring

Journal:	<i>Analyst</i>
Manuscript ID:	AN-ART-03-2015-000478.R1
Article Type:	Paper
Date Submitted by the Author:	16-Apr-2015
Complete List of Authors:	Nunes, Pedro; Technical University of Denmark, Department of Micro- and Nanotechnology Kjærulff, Søren; ChemoMetec A/S, Dufva, Martin; Technical University of Denmark, Department of Micro- and Nanotechnology Mogensen, Klaus; Technical University of Denmark, Department of Micro- and Nanotechnology; Technical University of Denmark, Dept. of Micro and nanotechnology

ARTICLE

Real-time direct cell concentration and viability determination using a fully automated microfluidic platform for standalone process monitoring

P. S. Nunes,^a S. Kjaerulff,^b M. Dufva^a and K. B. Mogensen^a

Received 00th January 2015,

Accepted 00th January 2015

DOI: 10.1039/x0xx00000x

www.rsc.org/

Industrial production of cells has a large unmet need for greater process monitoring, in addition to the standard temperature, pH and oxygen concentration determination. Monitoring the cells health through a vast range of fluorescence cell-based assays can greatly improve the feedback control and thereby ensure optimal cell production, by prolonging the fermentation cycle and increasing the bioreactor output. In this work, we report on the development of a fully automated microfluidic system capable of extracting samples directly from a bioreactor, diluting the sample, staining the cells, and determining the total cell and dead cells concentrations, within a time frame of 10.3 min. The platform consists of custom made stepper motor actuated peristaltic pumps and valves, fluidic interconnections, sample to waste liquid management and image cytometry-based detection. The total concentration of cells is determined through brightfield microscopy, while fluorescence detection is used to detect propidium iodide stained non-viable cells. This method can be incorporated into facilities with bioreactors to monitor cell concentration and viability during the cultivation process. Here, we demonstrate the microfluidic system performance by monitoring in real-time the cell concentration and viability of yeast extracted directly from an in-house made bioreactor. This is the first demonstration of using the Dean drag force, generated due to the implementation of a curved microchannel geometry in conjunction with high flow rates to promote passive mixing of cell samples and thus homogenization of the diluted cell plug. The autonomous operation of the fluidics furthermore allows implementation of intelligent protocols for administering air bubbles from the bioreactor in the microfluidic system; so that these will be guided away from the imaging region; thereby significantly improving both the robustness of the system and the quality of the data.

Introduction

Industrial production of cells (e.g.: bacteria, yeast, mammalian cells) in large-scale bioreactors is commonly controlled by automated measurements of the temperature, pH, and oxygen concentration, while other parameters as e.g. the cell biomass are still manually measured.¹ The additional ability to monitor in real-time the cell concentration and viability has been identified as an important feedback control during fermentation.²⁻⁴ Microfluidic technology has the well-known advantages of low reagents consumption, short analysis time, portability and increased fluidic control, among others, which is considered advantageous for cellular analysis.^{5,6} Thus, a microfluidic system that could be directly connected to a bioreactor, stain and dilute the cells to appropriate concentrations for imaging, determine the cell concentration, viability and cell health would considerably improve the feedback control of such a large-scale bioreactor and therefore allow an optimized performance.

Cell concentration and viability can be monitored using several methods, such as flow cytometry and image cytometry.^{2,7} State of the art devices capable of measuring yeast concentration and viability, using image cytometry-based detection are currently commercialized by Nexcelom Bioscience (USA)⁸ and ChemoMetec (Denmark)⁹. However, these methods currently require an operator to manually perform dilutions and fluorescently stain the cells. Manual sample dilutions are needed as bioreactors can achieve cell concentrations of more than 10^9 cells/ml¹⁰ and high cell concentrations ($> 10^7$ cells/ml) severely complicate automated image cytometry-based analysis, as the cells are too closely packed to be robustly segmented. To address this problem, cell samples extracted from a bioreactor should be diluted before performing image cytometry-based detection on chip.

The ability to mix liquids in microfluidic devices is uttermost important for a multitude of applications within chemical and biochemical analysis systems.¹¹⁻¹³ Microfluidic mixers can be categorized as either active or passive. Active mixers¹⁴⁻¹⁷ are typically not applicable when dealing with sensitive species as

1 cells. Passive mixers are based on carefully designed
2 microstructures and only rely on the force used to drive the
3 fluid flow. These enhance diffusion through chaotic advection
4 or by increasing the contact area and time between species.
5 Albeit mixing in microfluidic devices is a well-studied
6 problem, most publications only address the dilution and
7 mixing of small molecules or particles, e.g. color dyes,
8 fluorescent dyes,^{18,19} drugs,²⁰ particles,^{17,21} etc. Cells, due to
9 their large dimensions, have considerably low diffusion
10 coefficients, thus dilutions purely based on diffusion are not
11 applicable within typical microfluidic footprints. Furthermore,
12 as bioreactors start from low cell counts, a large range of cell
13 concentrations needs to be monitored. The problem of non-
14 diffusional mixing and homogenization of diluted cell samples
15 in a wide concentration range is underexplored in the field of
16 microfluidics. Only a limited number of works have been
17 published, where cell sample dilution is addressed^{22,23} and here
18 only up to 10 times dilutions were performed. We propose that
19 sheathing the cell stream using a diluent and subsequent
20 channel meandering exploiting Dean vortices will provide
21 necessary dilution on chip under adequate flow conditions.

22 For the current application within on-line process monitoring of
23 large-scale production of cells, the system to drive such a
24 microfluidic chip requires very precise pumping and valving
25 features in order to enable the ability to handle large volume
26 samples; multiple sampling; high precision and a high level of
27 automation. Multiple sampling creates a need for highly robust
28 and reversible valving mechanisms, in order to minimize the
29 number of pumps and the platform footprint. Some examples of
30 devices with integrated reversible valves include the use of
31 thermoresponsive ionogel²⁴ and PDMS micromechanical
32 valves,²⁵ however these have very limited lifetimes.
33 Furthermore, multiple sampling requires the means to analyze a
34 fresh cell sample within 10 to 15 min, thus operating flow rates
35 between one and hundreds $\mu\text{l}/\text{min}$ are preferred. Therefore
36 external pumping and valving were preferred in order to: a)
37 reduce the chip complexity, thus reducing the number of
38 structures where air bubbles can become trapped, b) achieve
39 high pumping precision, c) sustain high back pressures and d)
40 enable the implementation of automated protocols for
41 administering air bubbles.

42 In this work, we address a novel application dealing with
43 process monitoring of fermentation-based production using a
44 robust, accurate, self-contained and portable microfluidic
45 system, motivated by previously reported peristaltic
46 micropumps and valves.^{26,27} This system enables several
47 automated tasks, such as real-time sampling from a bioreactor,
48 cell dilution, staining, chip cleaning procedures and finally
49 image acquisition and analysis. The platform components were
50 carefully designed and optimized in order to sustain a wide
51 range of flow rates (5 - 700 $\mu\text{l}/\text{min}$) and dilution factors (10 –
52 260 times) in a highly reproducible manner, while
53 simultaneously enabling a high level of automation, thus
54 removing the necessity for user-input during operation.
55 Intelligent fluidic procedures were furthermore incorporated in
56 the automated protocol in order to significantly reduce errors
57 due to air bubbles in the ferment. Overall, the work reported in
58 this paper address the generally neglected aspects of
59 automation, reliability and error-control in order to meet the
60 requirements of user-friendly commercial systems, which is
61 recognized as a core requirement for the future of
62 microfluidics.²⁸

Design principle

The design of the dilution microfluidic chip is based on the adjustment of the flow rates provided by two individually actuated micropumps. The initial concentration of cells, C_i , is determined based on the dilution factor, α , and the measured final concentration of cells, C_f , which can be expressed as $C_i = C_f \cdot \alpha$, where α can be calculated from the ratio of the merging flow rates of the cell sample, Q_s , and the diluents, Q_d :

$$\alpha = \frac{Q_s + Q_d}{Q_s}$$

As cells have low diffusion coefficients, a simple Y inlet would lead to a laminated cell stream. In order to promote mixing and thus homogenization of the diluted cell population, a combination of hydrodynamic focusing and Dean vortices was exploited.

Dean vortices arise in the vertical plane of curved channels, due to the balance between inertial, centrifugal and viscous forces.¹⁸ The transverse secondary flow due to Dean effects can be characterized in terms of the dimensionless Dean number, De , where ρ is the fluid density (kg/m^3), U the average fluid velocity (m/s), D_h the hydraulic diameter (m), μ the fluid viscosity ($\text{kg}/\text{m}\cdot\text{s}$), R (m) the radius of curvature of the microchannel and Re the dimensionless Reynolds number.

$$De = \frac{\rho U D_h}{\mu} \sqrt{\frac{D_h}{2R}} = Re \sqrt{\frac{D_h}{2R}}$$

The hydraulic diameter of the channel can be calculated as $D_h = 4 \frac{A}{P}$, where A is the channel cross sectional area and P is the channel perimeter.²⁹ Low Dean numbers ($De = 1$) are not significant enough to perturb the laminar flow, however at $De > 10$, two counter rotating vortices are developed in the vertical plane perpendicular to the flow direction.¹⁸ As the axial velocity is highest at the centerline, so is the centrifugal effect, leading to a flow along the channel midplane towards the outer wall. In order to maintain mass balance the fluid closer to the sidewalls is pushed away from the wall, thus creating two counter rotating vortices.

The use of hydrodynamic focusing to laminate the cell sample on both sides by the dilution buffer, doubles the contact area in comparison to a simple Y inlet configuration, thus enhancing the mixing promoted by the generated secondary transverse Dean flow.

In this work, we take advantage of the system requirement for multiple sampling, to operate at high flow rates ($Re > 10$) in comparison to most microfluidic devices. This in combination with carefully designed microchannels enables sufficiently high Dean numbers to promote mixing and homogenization of the diluted cell sample. It is due to the robustness and precision of the custom made pumps and valves that the operation in this regime is possible.

Experimental

Fabrication principles

The microfluidic system components were fabricated mainly using computer numeric control (CNC) micromilling (Mini-Mill/3, Minitech Machinery Corporation, USA) for depth dependent structures and laser ablation using a CO_2 laser (Epilog Laser 30 Watts, USA) for depth independent structures. The components were typically assembled using 2 mm screws and respective nuts, to ensure the reversibility of the connections made.

ARTICLE

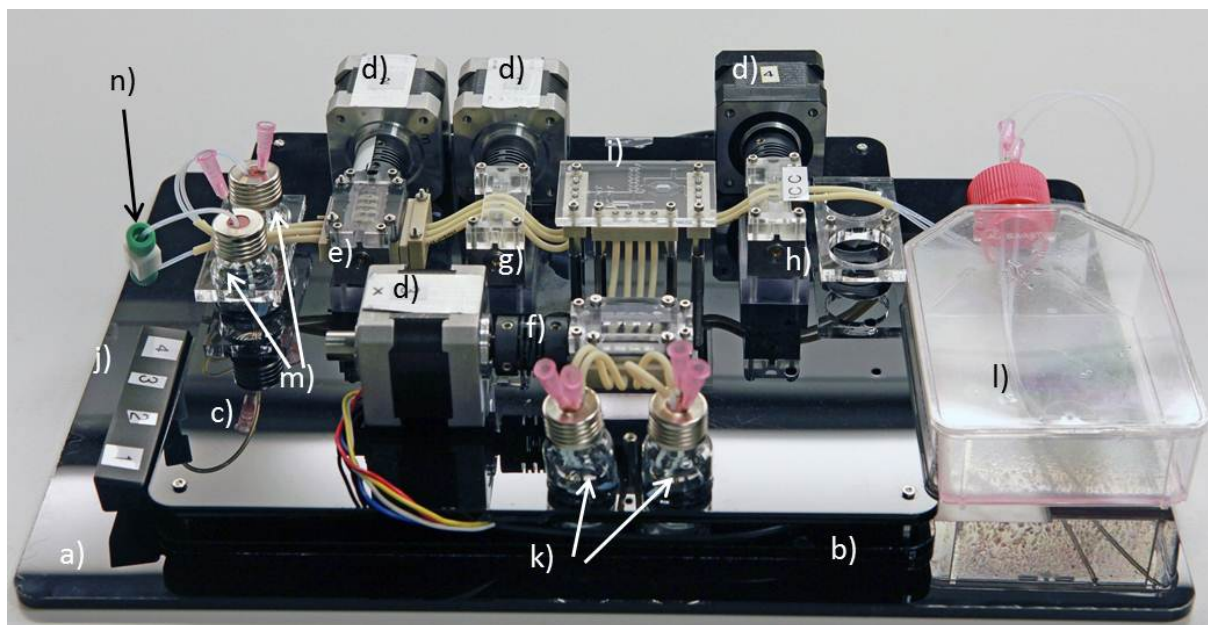


Figure 1 - Microfluidic platform consisting of: a) Bottom black PMMA plate, b) Middle black PMMA plate, c) top black PMMA plate, d) stepper motors, e) multi-channel peristaltic pump for pumping cell samples and washing buffer into the chip, f) multi-channel peristaltic pump for pumping the dilution buffer, g) multi-channel valve for fluid routing, h) outlet multi-channel valve, i) microfluidic chip, j) USB connectors for controlling the stepper motors, k) dilution buffer reservoirs, l) waste reservoir, m) washing buffer reservoir, and n) high pressure fitting for connecting to the bioreactor.

System base

The system components are assembled on three black poly(methyl methacrylate) (PMMA) plates (5 mm thick), Figure 1 a-c). The bottom PMMA plate has a hole through, which fits around the microscope stage, thus enabling the system to be easily removed and re-aligned.

The middle base plate rests on top of the microscope stage and the bottom PMMA plate and is separated from the top baseplate by 10 mm spacers (BS-L10-TA-M2, Toby Electronics, UK), in order to accommodate the electrical cables connected to the stepper motors, as well as the USB interfacing port, Figure 1 j).

The top base plate supports four computer controlled stepper motors, Figure 1 d), two multi-channel peristaltic pumps, Figure 1 e) and f), two multi-channel valves, Figure 1 g) and h), two 4 ml glass vials for storing the washing buffer, Figure 1 m), two 4 ml glass vials for storing the dilution buffer, Figure 1 k), and a 160 ml waste reservoir, Figure 1 l). The system has a footprint of 220 mm x 250 mm x 77 mm.

Multi-channel micro peristaltic pump

The multi-channel peristaltic pumps developed and implemented in this platform have been motivated by a previously described design.²⁶ The current micropump differs from a previous version both in terms of components and design, in order to fulfill the need for a wide flow rate range and robustness. The micropump, as shown in Figure 2 can be characterized in terms of three main components: 1) a multi-

roller; 2) a rotor bed, and 3) heavy duty pump tubing, where 1) and 2) were micromilled.

The current micropump is actuated by high precision stepper motors (MP042NB340 Rev P2, 1.8°/step, GCM A/S, Denmark), Figure 2 c). Peristaltic pumping is achieved when the rotor bed occludes the highly resistant commercial micropump tubing (RCT-ISMT-1-TPE #339983, RCT, Germany) with an inner diameter (ID) of 0.76 mm between the multi-roller rolling pins and its lower surface. In order to accommodate the larger micropump tubing the curvature of the rotor beds lower surface was modified. Care was also taken in order to decrease the friction between the three main components, by increasing the distance between the multi-roller and the rotor bed, but still ensuring reproducible peristaltic pumping.

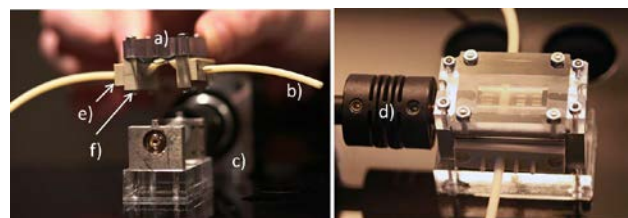


Figure 2 - Peristaltic micropump consisting of a) rotor bed, b) heavy duty pump tubing, c) stepper motor, d) plastic coupling to stepper motor, e) tube to tube fluidic interconnections and f) brackets for fastening the tube to tube interconnections to the tubing.

This greatly contributes to decrease the need for high torque motors and to avoid components from unnecessarily wearing off.

Extra alignment structures were introduced in the rotor bed to accommodate the fluidic interconnections, Figure 2 e) and f), in a way that the tubing can always be assembled, even when the micropump is removed from the platform.

The multi-roller in earlier versions consisted of eight free-rolling 2 mm stainless steels pins, however in the current version these were decreased to four pins, thereby decreasing the number of pulses per revolution, as well as increasing the pumped volume per revolution.

Multi-channel micro valve

The multi-channel micro valve design and fabrication is built on the knowledge used to develop an earlier previously described version,²⁶ but it was considerably modified, as the earlier designs were not robust enough for long term operation and automation. The valve consists of a camshaft, a tubing holder and a lid, Figure 3. The camshaft consists of four individual cams, micromilled in polyether ether ketone (PEEK), which are assembled along a central 4 mm wide brass shaft and two 2 mm wide alignment pins, Figure 3 a). The tubing holder was fabricated through CNC milling in PMMA and consists of four parallel circular through holes ($\phi = 3.1$ mm), below each of the four ridges, used as guides for the micropump tubing, Figure 3 b). The valve lid rests on top of the tubing holder keeping the tubes in place, Figure 3 c). Two 3 mm stainless steel spheres (3.0 mm spheres, Carl Hassing, Denmark) are placed in each of the circular through holes of the tubing holder, Figure 3 d). Valving is achieved by rotating the camshaft, thus pressing the spheres against the tubing, due to the cams profile. The height of the tubing holder is set so that the 3 mm spheres are always kept inside the circular holes, and when the depressions in the cam are aligned with the spheres the tubing is fully opened, by allowing the spheres to descend 1.2 mm. The cams were designed with depressions or protrusions spaced by 90° in a total of four possible positions per cam. Prior to operation, the cams are assembled in a predetermined position, calculated based on the intended fluidic operations.

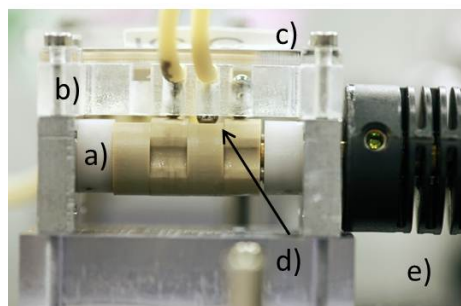


Figure 3 - Multi-channel valve consisting of: a) camshaft, b) tubing holder, c) lid, d) 3 mm stainless steel spheres and e) plastic coupling to the stepper motor.

Fluidic interconnections

Two different types of fluidic interconnections were designed: tube to chip interconnections and tube to tube interconnections. The tube to chip interconnections, Figure 4 a), consist on the side facing the tubing, of hollow cylinder structures 5.37 mm long (0.37 mm high dome), which are press-fitted into the heavy duty tubing. These have an ID of 0.8 mm and outer

diameter (OD) of 1.3 mm, spaced apart by 4.5 mm, with a total of four connections. Both ends of the connector have a hexagonal pocket (2 mm deep) designed to fit tightly around the hexagonal spacers used to raise the chip from the black PMMA plate. The opposite side of the connector has dome like structures with an ID of 0.8 mm and an OD of 1.45 mm, with a total height of 0.8 mm and with a dome height of 0.4 mm. This tube structure lies over 3 mm wide and 1 mm high cylinder, over which an o-ring is placed (OR 1.00 – 0.50 NBR70, MSeals, Denmark). The o-ring ensures that there is no leak between the connector and the chip inlet/outlet. This connector has an 8 mm x 30 mm x 8 mm (w x l x h) footprint.

The tube to tube connections, Figure 4 b), which are solely used in the peristaltic pump inlet and outlet, Figure 4 e), consist of a duplicate of the long tubes of the tube to chip connector on both sides of the tube to tube connector, yielding a total connector footprint of 8 mm x 30 mm x 12 mm (w x l x h). The actuation of the peristaltic pump promotes the tubing to move slightly in the direction of the actuation. The tubing movement per revolution is insignificant; however in continuous operation this may lead to the detachment of the tubing from tube to tube connector. To ensure that the system is full leak proof, two brackets are placed on each side of the tube to tube connector, as shown in Figure 4 c). These are then fastened to the rotor bed, Figure 2 e) and f). The fastener has a footprint of 5 mm x 30 mm x 5.8 mm (w x l x h) and 1 mm deep, 2.8 mm wide and 5 mm long trenches separated by 4.5 mm.



Figure 4 - Fluidic interconnections. a) Tube to chip interconnections, b) Tube to tube interconnections and c) Brackets for fastening the tube to tube interconnections to the tubing.

Peripheral components

An in-house built control box powered by an external power supply contains a PCB board (NC2-Backplane v1.02, ChemoMetec A/S, Denmark) capable of interfacing up to six stepper motor drivers, as well as providing digital output signals, which were used to trigger the acquisition camera interfacing the microscope. The stepper motor driver boards are connected to female USB ports, as well as the stepper motors controlling either the pumps or the valves. Connection between them is established by a standard USB cable extension.

Software control

Actuation of the stepper motor controlled peristaltic pumps and valves is made through an FDTI terminal (ChemoMetec A/S, Denmark), where the motors RPM and the number of steps can be adjusted, as well as triggering of the camera for timed image acquisition through the microscope.

Chip design and fabrication

Fluidic simulations using the numerical finite element method (FEM) were implemented in Comsol Multiphysics (Comsol 4.3b, Comsol AB, Sweden). A 2D FEM model combining an incompressible Navier-Stokes model (laminar flow) with a convection-diffusion model in steady state is used to determine a suitable channel geometry for the proper merging of the highly different flow rates of Q_s and Q_d , in order to prevent

significant backflow. The boundary conditions for the Navier-Stokes model include a no-slip condition at the sidewalls, laminar inflow flow rate at the inlets and pressure with no viscous stress at the outlet. The convection-diffusion model was defined by specifying the concentration of the species of interest at the inlet, using a diffusion coefficient of 10^{-12} m²/s for simulating large molecules, and by applying no-flux symmetry at the sidewalls and convective flux at the outlet. The microfluidic chips are fabricated in three layers of PMMA, Figure 5 a-c). The top layer is 0.5 mm thick in order to reduce the optical path length, between the microscope objective and the imaging chamber. The middle layer is 2 mm thick in order to provide a certain degree of rigidity to the chip, while the bottom layer is 1 mm thick.

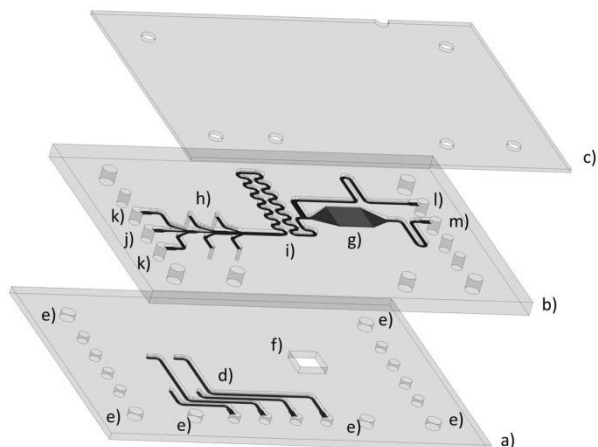


Figure 5 - Exploded view of the three layered microfluidic chip: a) bottom layer, b) middle layer, c) top layer. The bottom layer consists of: d) four inlets with channels (cross section: 0.5 mm x 0.5 mm); e) through holes for M2 screws and f) a square through hole. The middle layer consists of: g) an imaging chamber (5 mm x 5 mm x 0.1 mm); h) four through holes for microfluidic connection with the bottom layer; i) a serpentine structure used for mixing as well as a reservoir; j) an inlet for cells; k) two inlets for washing buffer; l) an outlet channel not passing through the imaging chamber and m) the imaging chamber outlet.

The middle and bottom layer were fabricated with CNC micromilling, while the lid was laser ablated. In order to ensure low surface roughness during milling a mixture of water and mild detergent was used as a lubricant. However, for achieving a high quality imaging surface, mineral oil was used as a lubricant. The three layers were subsequently sonicated for 15 min in a solution of water and mild detergent. The layers were then rinsed with IPA, Milli-Q water, subjected to chloroform fumes for 1 min for chemical smoothing and then rinsed with Milli-Q water. Prior to bonding the substrates were surface activated in a UV chamber (Dymax, 5000 EC, USA). Following the UV exposure, the layers were stacked, aligned with 2 mm wide rubber pins, Figure 5 e), placed between two glass slides and bonded for 35 min at 80 °C with an initial bonding pressure of 8 kN in a bonding press (PW 10 H, P/O/Weber, Germany).

The middle layer of the chip in Figure 5 b) consists of a serpentine mixing structure (h: 0.5 mm, w: 0.5 mm, l: 51 mm, 12.8 μ l), an imaging chamber (h: 0.1 mm, w: 5 mm, l: 5 mm, vol. 2.5 μ l), two inlets for the washing buffer, one inlet for the cell solution, an outlet that bypass the imaging chamber and finally the outlet of the imaging chamber. Both the inlets and outlets consist of 1.5 mm wide through holes with a distance of 4.5 mm in order to fit to the developed tube to chip

interconnections, Figure 5 a). The bottom layer of the chip in Figure 5 a) consists of four standard inlet holes and channels (h: 0.5 mm, w: 0.5 mm) connected to both sides of the central channel in the middle layer via 0.5 mm wide through holes. Both inlets and outlets are connected to the bottom chip layer, in order to facilitate the imaging acquisition of different areas of the chip.

The chamber depth after milling was measured using a profilometer (Alpha-step IQ, KLA-Tencor, USA). To ensure that there is no collapse of the chamber lid after bonding, the chamber depth was also determined by measuring the absorbance of a 1 mM aqueous solution of bromothymol blue in the chamber using a spectrophotometer (UV-1800, Shimadzu, Japan).

Flow characterization

The flow rate for each channel in each pump was determined using anemometry volume flow meters (Mitos Flow Rate Sensor, Dolomite, UK) for 2 different flow rate ranges 1 - 50 μ l/min and 30 - 1000 μ l/min. The individual inlets of the peristaltic pumps were connected via PTFE tubing (ID 0.8 mm and OD 1.6 mm; BOLA 1810-10, Bohlender GmbH, Germany) to a 4 ml glass vial with tight sealed screw cap containing Milli-Q water. The glass vial cap had an additional hole used as an air vent in order to ensure the solution was continuously at atmospheric pressure. The outlets of each pump were also connected to PTFE tubing by high pressure fittings (IDEX Health & Science, Germany), which interfaced the flow meter. The flow rate from the peristaltic pumps is inherently pulsating, therefore two 4 ml glass vials with tight sealed screw caps were inserted in series between the pump and the flow rate sensor to ensure a steady flow. These were pre-filled with 2 ml of Milli-Q water.

A script was written in the FDTI terminal where for each channel the RPM of the stepper motor actuating the peristaltic pump was varied between 1 and 120 RPM in random order and each cycle ran 5 times. Between each analyzed RPM, an interval of 2 min was introduced in order to ensure that the measured flow rate would drop to 0 μ l/min.

The data analysis was performed using a custom-made program written in Matlab R2014a (MathWorks, USA), where the flow rate for each RPM is extracted from the data logged with a sampling frequency of 1 Hz (Mitos Flow Control Center, vers 2.2.13 software). In order to ensure that the flow rate provided by the micropump was not altered, when the valve was inserted in the system (in an open configuration), the flow rate was once again characterized as described previously, but in this case the tubing coming out from the peristaltic pump was passing through the valve and then connected to the PTFE tubing.

Optical setup, image acquisition and analysis

The optical setup consists of an upright microscope (Axio Imager M1.m, Carl Zeiss, Germany) equipped with a camera from Oxford Instruments (Neo sCMOS Andor Technology, Oxford Instruments, UK). The microscope can be both used for brightfield, as well as fluorescence imaging. Imaging of propidium iodide stained cells (λ_{exc} = 535 nm and λ_{em} = 617 nm) was achieved by using an adequate filter cube (Cube set 43 He, Carl Zeiss, Germany), which consists of the following filters: BP 550/25, dichroic mirror FT 570 and BP 605/70. A 5x magnification objective (Zeiss A-plan 5x, Carl Zeiss, Germany) was used for image acquisition. Image acquisition was performed by running a custom made script in the Andor Solis (Andor Solis for Imaging, vers. 4.22.30007.0), in order to

specify the exposure time and record images when the external PCB board triggers the camera. The image analysis was performed using a custom-made program written in Matlab R2014a, based on the available Image-based Tool for Counting Nuclei (ITCN) [25]. The available ITCN script is able to rather accurately analyze fluorescence images. However, when using a low magnification (5x) a large area is imaged and therefore it is more susceptible to the inhomogeneity of the mercury light source. Thus, prior to running the ITCN script, the contrast of the images was increased and the background subtracted; such a script will be referred as CellAutoFL. The automated brightfield image analysis script consisted of inverting the original brightfield image, increasing the contrast, subtracting the background, increasing the contrast and finally inverting the image and then running the ITCN script. This will be referred to as CellAutoBF.

Yeast cultivation and fermentation

Yeast, *Saccharomyces cerevisiae*, was supplied by ChemoMetec A/S, Denmark. The yeast was grown in YPD broth (Y1375, Sigma-Aldrich) in a home-made bioreactor agitated by magnetic steering (IKA RCT basic, from Bie & Bernsten). The bioreactor consisted of a 400 ml bottle with a teflon screw cap with three through holes for accessing the solution, as well as for proper aeration. One hole was connected to a mini sterile filter 0.2 μm (Minisart, Sartorius Stedium Biotech, Germany). The other two holes were used for manual and automated solution sampling.

The manual sampling was performed via a PTFE tubing (ID 0.8 mm and OD 1.6 mm) connected on the external end to a high pressure fitting and to a Luer adapter via a thread port adapter (I dex Health & Science, Germany). For manual sampling a 5 ml syringe with a Luer lock (Injekt 5 ml, B. Braun, USA) was connected to the adapter and approximately 1 ml of sample was extracted from the bioreactor. After removal of the syringe, the PTFE tubing was connected to a 0.2 μm sterile filter (Minisart, Sartorius Stedium Biotech, Germany) and purged with air, which enabled aeration of the solution. The other end of the PTFE tubing was mounted in a fixed position in approximately the center of the bioreactor to ensure reproducible sampling. The automated sampling was performed similarly to the manual sampling. However, the PTFE tubing on the external end was press fitted into the micropump tubing connected to the microfluidic system.

Yeast concentration and viability

The control measurements were performed using the NucleoCounter NC3000 (Assay number 994-3031, ChemoMetec A/S, Denmark).⁹ Enumeration of viable and dead cells was determined according to the manufacturer's instructions. Briefly, the samples extracted manually from the bioreactor were diluted up to 10 times in a 0.05 M Tris buffer (T6664, Sigma-Aldrich) depending on the cell concentration. To determine the total concentration of cells, these were incubated in a lysing solution (Y100, ChemoMetec A/S, Denmark) for 10 min. The solution prior to the addition of Y100 was used to determine the concentration of dead cells.

The concentration of dead cells was measured in the microfluidic system by propidium iodide staining using the following solution: 0.05 M Tris buffer supplemented with 20 $\mu\text{g}/\text{ml}$ propidium iodide (ChemoMetec A/S) and 0.05% Tween-20 (P9416, Sigma-Aldrich). This solution was used for performing the sample dilution and cell staining in the

microfluidic chip. A solution of 0.1 M NaOH was pumped into the chip and used for washing and chemical sterilization.

The process flow in the microfluidic system can be divided in three distinct scripts, which are run in cycles (Table 1). In the first script, the tubing connecting the peristaltic pump to the bioreactor is re-filled with a fresh solution of cells (s_1), while in the second script the chip is cleaned with a solution of 0.1 M NaOH, for removing any cells from the chip and most importantly from the imaging chamber (s_2).

In the third script a plug of the yeast sample is diluted and stained with PI. Five consecutive sub plugs, within the initial plug are imaged using both brightfield field and fluorescence detection (s_3). The cycle finishes with an additional cleaning script (s_2).

For monitoring the cell growth, intervals of 20 – 30 min were chosen between each cycle. Three dilution factors were used, yielding a 10 times dilution factor ($s_{3_{10}}$), an 88 times dilution factor ($s_{3_{88}}$) and a 259 times dilution factor ($s_{3_{259}}$). For simplicity the scripts combination s_1 , s_2 , $s_{3_{ii}}$ and s_2 , will be referred as S_{ii} . For further information regarding the experimental setup see the supporting information.

Script (time)	Goal	NaOH vol.	Cell vol.	Q_s	Dilution buffer vol.	Q_d
s_1 (112sec)	Re-fill cell tube	1581.0	937.7		251.6	
s_2 (110 sec)	Cleaning	392.9	-	-	-	-
$s_{3_{10}}$ (288sec)	Detection	-	122.0		119.5	-
	Dil. Plug	-	6.7	54.5	58.3	119.0
$s_{3_{88}}$ (288 sec)	Detection	-	120.4		325.5	-
	Dil. plug	-	3.0	5.5	256.8	119.0
$s_{3_{259}}$ (288 sec)	Detection	-	123.4		903.1	-
	Dil. plug	-	3.3	5.5	843.0	354.0

Table 1 - Process flow scripts and respective time (sec). Flow rates expressed in $\mu\text{l}/\text{min}$. Volumes expressed in μl .

Results

Pump characterization

A key factor when evaluating a multi-channel pump is the variability between the channels, the stability of the flow rate in time, and the variability between pumps. The flow rate was measured in a high speed mode (operating the diluent) and a low speed mode (drawing samples from the bioreactor) using two different flow rate sensors. In both cases, a linear correlation was obtained between the pump rotational speed and the obtained flow rate, as expected (Figure 6). The relative standard deviation was low (< 3%) except when the measurement was done near the respective flow rate meters lower limits (30 $\mu\text{l}/\text{min}$ and 1 $\mu\text{l}/\text{min}$ respectively).

The pump durability was tested at a high rotational speed (90 RPM), yielding a flow rate of $524.4 \pm 20 \mu\text{l}/\text{min}$, which corresponds to a relative STD of 3.8 %. This test consisted of 900 cycles of 6 min, where Milli-Q water was pumped for 3 min with a 3 min interval between cycles, corresponding to a total pumped volume of 1.4 L over 90 hrs of continuous operation (243,000 micropump rotations), when the test was voluntarily stopped.

It was further observed that the performance of the pump has not significantly changed during several months of use, however data has not been recorded continuously.

ARTICLE

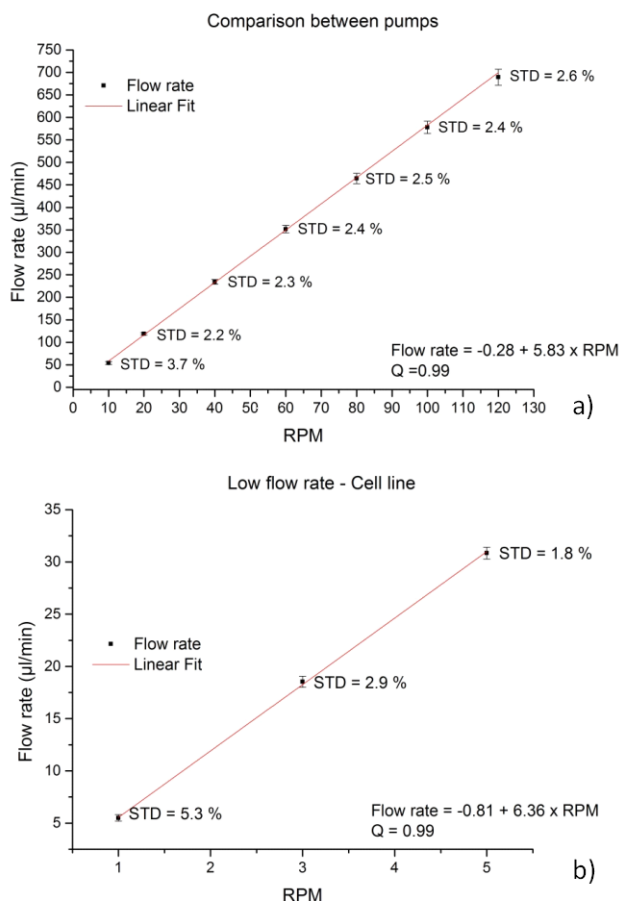


Figure 6 – a) Reproducibility between pumps. b) Flow rate calibration curve for the cell line. The error bars correspond to 5 data points.

Multi-channel valve performance

The valve performance was characterized based on its ability to block the flow in the individual channels independently of the expected flow rate provided by the micropump and by not altering the flow rate provided by the micropump when the valve channels are open. A major concern was the pressure built up when the pump was actuated at high rotation speeds (90 RPM – 524 µl/min) and the valve channels were closed. Despite the initial concerns no leaks were observed, and it was observed that this pressure was partially relieved by a back flow in the micropump. This observation was possible by introducing an air plug in the micropump inlet tubing, 10 cm away from the micropump, and noticing that these were pushed forward and backward, due to the forward piston movement in the pump and the release of the void created by the piston in the tubing, respectively. Such a test also proved that the developed fluidic connections sustain high pressures. The valve was actuated at 120 RPM, which enables addressing each of the

four positions in each valve cam within less than 0.13 s. Upon release of each tubing, a small burst of fluid was observed due to release of the built up pressure. Valve durability tests were performed by actuating the valve at 120 RPM over 50,000 rotations, where one rotation corresponds to one valve position. After the test it was observed that the valve positions were still aligned with the circular holes in the tubing holder and that the tubing had not become damaged. The flow rates and their relative STD measured when the valve was included in the flow characterization circuit were the same as when no valve was present (data not shown). This was expected, as visually the tubing was not compressed in the valve.

Chip design and simulations

In order to monitor yeast growth from 10^5 up to 10^9 cells/ml it would be necessary to perform dilutions up to 260 times and the chip was therefore designed to accommodate this range of dilutions.

The home-made bioreactor could, however, only reach a concentration of 10^8 cells/ml, due to limitations in the fermentation apparatus. Performing large dilutions with the current method of individually adjusting the flow rates of the sample and of the diluent creates large differences in the necessary flow rates, which may lead to high backpressures. This could prevent the cells from being diluted, or contaminate the surrounding channels with foreign species. E.g. for performing a 259 times dilution and assuming a flow rate for the cell sample of 5.5 µl/min, a flow rate of 1419 µl/min for the dilution buffer would be necessary. Such a high flow rate has not been measured, but based on the linear fit for our flow rate measurements it would imply actuating the peristaltic pump at 243 RPM. Even though possible, it would lead to an increased friction and degradation of the components. It is possible to reduce the necessary flow rate per channel to 355 µl/min (with a pump actuation of 60 RPM) by separating the dilution buffer flow rate into four individual channels. Figure 7 a) and b) illustrates that when the flow rates are significantly different, there is a backflow in the central channel (marked with i), which leads to an increase in the expected dilution factor. Therefore the final microfluidic device consists of four inlet channels for the dilution buffer connected to the central channel on both sides.

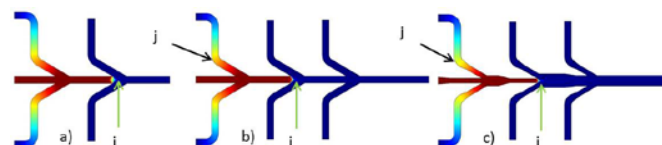


Figure 7 - Comsol simulations of the sample concentration. The red color corresponds to a normalized sample concentration of 1, while the dark blue corresponds to 0. The sample flow rate was 5.5 µl/min, while the washing buffer flow rates was 0 µl/min. a) Diluents flow rate of 708 µl/min per channel. b) Standard channels width 0.5 mm and diluents flow rate of 354 µl/min per channel. c) Restricted channels width and diluents flow rate of 354 µl/min per channel (see supporting information for more details).

The microfluidic chip is intended as a multiple-use device, so the channels geometries have to be designed to facilitate the cleaning of the chip, as well as to prevent foreign species from entering the surrounding channels. By reducing the width of the inlet channels, the fluidic resistance can be increased, thus preventing species from entering the surrounding channels, marked with j in Figure 7 b) and c). The final design consisted of a 0.350 mm restriction in comparison to the initial 0.5 mm wide channel, which was motivated by the preference to use the same milling tool used to fabricate the microfluidic chips middle layer.

The latter two pairs of lateral inlets used for the dilution buffer lead to a focused stream containing cells in the center of the microfluidic channel. However, as cells have insignificant diffusion coefficients a meandering channel was used to enhance mixing, thus homogenizing the diluted cell sample. Increasing the fluid velocity leads to stronger Dean vortices in curved channels, which in turn promotes mixing as the cells are entrained in the vortices.

The three dilution factors implemented in the current system are performed with a total flow rate of 531, 482 and 1422 $\mu\text{l}/\text{min}$, corresponding to the 10, 88 and 259 times dilutions. The Reynolds number in the serpentine channel are calculated to be 18, 16, and 47, leading to the following Dean numbers (curvature radius $R = 0.65$ mm): 11, 10, 29 for 10, 88 and 259 times dilutions, respectively.

The timescale associated with axial transport can be expressed as $t_a = L_a \cdot U_a$, where L_a and U_a correspond to the axial length and the axial fluid velocity, respectively. Similarly, the transverse transport timescale $t_D = L_D \cdot U_D$, where L_D and U_D correspond to the transverse migration length and the Dean fluid velocity, respectively. By setting the ratio of the corresponding timescales to 1, the transverse migration length can be expressed as $L_D = L_a \frac{U_D}{U_a}$. Here, the Dean fluid velocity in a channel with an aspect ratio close to 1 can be expressed as $U_D = 1.8 \times 10^{-4} \text{De}^{1.63} \text{ m/s}$.³⁰

Thus, the migration length perpendicular to the flow direction (L_D) for each turn ($L_a = 2.05$ mm) of the serpentine channel is calculated to be 0.51, 0.48 and 0.96 mm, corresponding to 10, 88 and 259 times dilution. As cells entrained in the vortices circulate at the velocity U_D along the circulation path with an estimated length equal to $D_n \frac{3}{2}$,³⁰ then a rotation of 248° , 233° and 461° is expected per serpentine turn. Visual observations of fluorescently stained cells in the serpentine channel show that the cells become well dispersed throughout the channel cross section after two to three serpentine turns. This was later confirmed by a well distributed cell population in the imaging chamber.

Image analysis validation

The chambers of 12 NucleoCassettes were imaged in order to validate the brightfield and fluorescence image analysis programs custom made in Matlab, by direct comparison with the results provided by the NucleoCounter NC3000. In this way, it was possible to get an accurate assessment of the image analysis performance, independently of fluid manipulations and the quality of the imaged surface. Examples of the custom image analysis programs are provided in the Supporting information.

Fluorescence images due to their low background noise are expected to be equally well analyzed by our method as by the NC3000 image analysis algorithm. In fact, the relative deviation between our method for determining the

concentration of stained cells [$c_{\text{CellAutoFL}}$] and the NC3000 [c_{NC3000FL}] is:

$$\frac{[c_{\text{NC3000FL}}] - [c_{\text{CellAutoFL}}]}{[c_{\text{NC3000FL}}]} < 1 \%$$

However, while the NC3000 calculates the total cell concentration using fluorescence, the CellAuto platform determines the total cell concentration using brightfield and the concentration of dead cells using fluorescence. In the NC3000 the cell sample is diluted 10 times in a lysing solution, thus all the cells will be stained with propidium iodide and not only the dead ones. Fluorescence images are more suitable for cell counting than brightfield images, since other debris, defects in the chamber surface or even clustered cells can influence the analysis of a brightfield image. Therefore, a larger deviation $< 5\%$ is obtained between the total cell concentration provided by the NC3000 [c_{NC3000FL}] and the one provided by CellAuto [$c_{\text{CellAutoBF}}$].

Platform dilution performance

A sample of stationary phase yeast cells was seeded in the bioreactor. The total concentration of cells measured by the NucleoCounter yielded $6.67 \pm 0.29 \times 10^6$ cells/ml (STD = 4.2 %), corresponding to the control measurements in Figure 8.

In order to validate the dilution factors, as well as to validate the automated image analysis, the total cell concentration in the bioreactor was measured for each dilution factor by running scripts S10, S88 and S259 consecutively three times (Table 1), as can be seen in Figure 8. The c_{tot} measured using the scripts S10, S88 and S259 yielded the following results $6.41 \pm 0.48 \times 10^6$; $6.58 \pm 0.41 \times 10^6$; and $6.53 \pm 0.31 \times 10^6$ cells/ml, corresponding to 7.6 %; 6.3 % and 4.8 % relative STD, respectively.

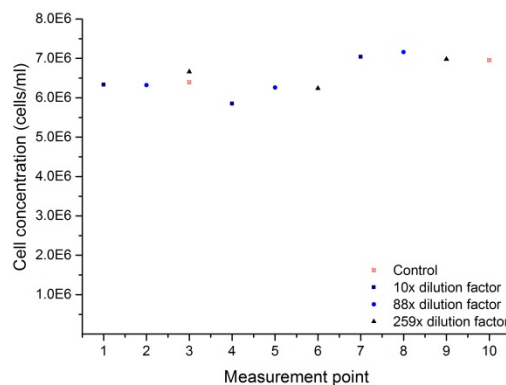


Figure 8 - Total cell concentration in the bioreactor measured for different dilution factors of the platform.

The scripts used for making the 10, 88 and 259 times dilutions include a subscript for cleaning the chip, by purging the chip with 0.1 M NaOH, thus removing cells present in the microfluidic channels, as well as in the imaging chamber. To prove that the cleaning scripts were efficient, images using brightfield and fluorescence of the imaging chamber prior to filling the chamber with the diluted cell sample were recorded. These images showed that no cells were sticking to the bottom surface of the chamber, thus proving the suitability of the cleaning script and cleaning buffer. However, if cells were left

Analyst

to sediment for more than 24 hrs, then the microfluidic chip would have to be discarded.

The diluted plug volume is 846 μl for the high dilution factor (259 times). Such a large volume would lead, even though rarely, to an air bubble trapped in the slope area, which would compromise the performance of the platform and hence complicate the overall goal of continuous monitoring of fermentation processes. The development of intelligent procedures for reducing errors is of major importance in order to ensure the reliability of the microfluidic systems and to guarantee the quality of the measurements. This is too often overlooked in the sense that the vast majority of chip protocols rely on a standard procedure that is carried to the end, no matter what happens along the way. To address this important issue, an additional script was written, so that when an air bubble is observed in the intersection, a volume of 3 μl is pumped into each of the seven inlet channels, while the outlet valve is closed. This creates an overpressure in the system, which leads to the collapse of the bubble and upon opening the valve, to flushing out of the bubble. By this simple procedure, the system is able to autonomously act on the specific situation, which ensures the ability of the platform to cope with continuous operation even in the presence of bubbles.

A mild surfactant (Tw20) was added to the dilution buffer in order to change the surface tension and hence further minimize the bubble trapping effect in the sloped intersection between the mixing channels and the imaging chamber. Surfactants are known to be used for chemical lysing of cells, thus different concentrations of Tw20 were tested using the lower dilution factor in the platform (S10). Dilution buffers containing 0.01 and 0.025 % (w/w) of Tw20 were insufficient to promote reproducible bubble removal from the chip, while 0.05 and 0.1 % were always capable of promoting the bubble release from the chip. The addition of 0.05% Tween-20 to a suspension of yeast cells had no influence on the viability within the time frame of the automated analysis (3 min) and demonstrated that low concentrations of the surfactant does not cause cell lysis (data not shown).

Figure 8 illustrates the performance of the entire microfluidic platform, including: a) the stability of the flow rates provided by the peristaltic pumps, b) the ability to route fluids by valve actuation, c) the adequacy of the fluidic interconnections, d) the microfluidic chip design, e) the scripts used for extracting a cell sample directly from the bioreactor, for cleaning the chip and for diluting the cell sample and d) the automated image acquisition and image analysis in a series of nine consecutive measurements, without observing any leaks or trapped bubbles.

Fermentation process monitoring

To prove the performance of the system in a situation that resembles as close as possible the intended operation, the yeast concentration and viability were measured during fermentation in a home-made bioreactor. The bioreactor was inoculated with yeast cells at an initial concentration of 1.0×10^5 cells/ml and growth was monitored for 21 hours.

Figure 9 illustrates the ability to monitor a wide range of cell concentrations (10^5 to 10^8 cells/ml), however due to limitations in the fermentation apparatus higher cell concentrations could not be achieved.

Both the lag and log phase were monitored using a 10 times dilution factor in 30 min intervals. The deceleration phase was monitored using 88 times dilution, also in 30 min intervals, in order to ensure that the cells in the imaging chamber can be individually distinguished.

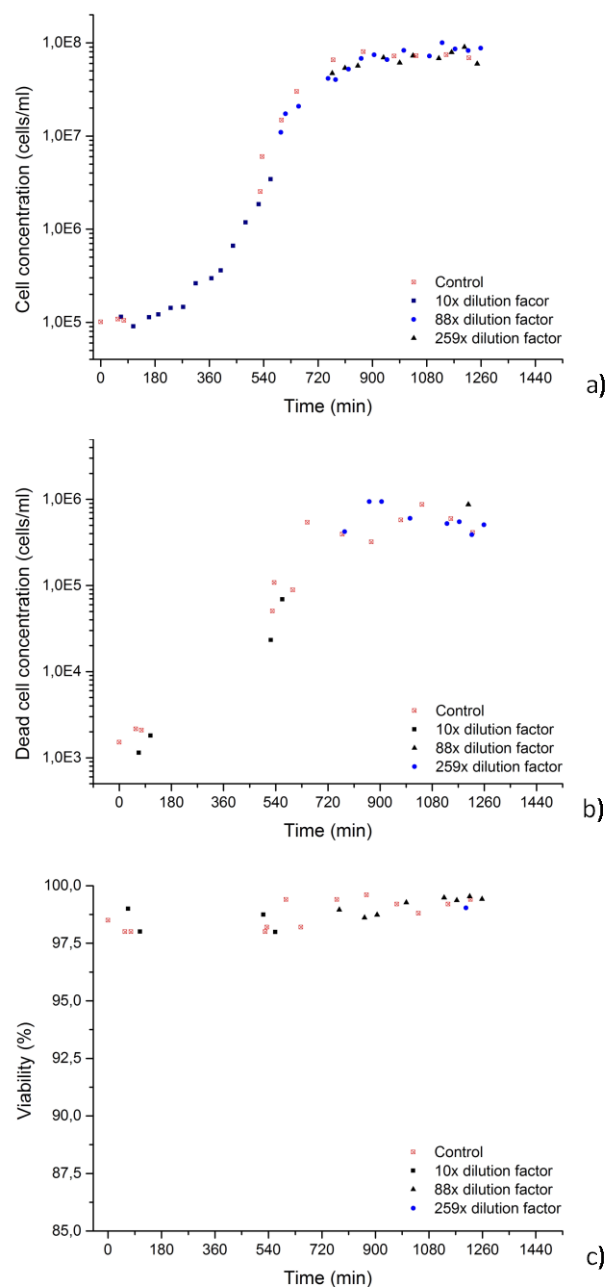


Figure 9 – a) Yeast growth curve using the CellAuto platform, obtained by analyzing brightfield images. Control measurements were performed using the NucleoCassettes in the NC300. Three dilution factors (10, 88 and 259 times) were used depending on the initial cell concentration. b) Dead yeast cells concentration. Fluorescence images of dead yeast cells stained with PI were acquired at the same time as the brightfield images. c) Yeast cells viability (%).

In the stationary phase, the cell concentration was monitored using 88 and 259 times dilutions, consecutively. Performing consecutive measurements enables a direct comparison of the calculated cell concentrations between the manually performed control measurements and the two dilution factors.

The dilution buffer serves two purposes. On the one hand, it is used to dilute the cell sample and on the other hand it also contains propidium iodide, which is used to stain dead cells.

Therefore, to monitor the concentration of dead cells (Figure 9 b), fluorescence images were acquired at the same time as brightfield images. The viability of the cell sample can be calculated based on the concentration of dead cells, as seen in Figure 9 c). As expected, a high cell viability was measured throughout the growth curve. Furthermore, Figure 9 c) illustrates that the viability of the yeast cells passing through the several components of the automated platform (e.g. peristaltic pump, valve, microfluidic chip, tubings) is not altered in relation to the manually performed control measurements.

Cell staining occurs instantaneously as the stained cells can be visualized along the serpentine structure used both for mixing as well as a reservoir, enabling several plugs to be imaged within one single dilution step.

Figure 9 illustrates a good agreement between the control measurements and the concentration values determined using the developed platform.

Discussion

Microfluidic systems have mainly been developed and used in an academic environment and have not been adopted as widely as expected in commercial settings due to the complexity of the systems and a general lack of reliability.^{28,31,32} The work reported in this paper addresses the generally neglected aspects of automation, reliability and error-control in order to meet the requirements of user-friendly commercial systems, which was emphasized by Whitesides as a core requirement for the future of microfluidics.²⁸

Saccharomyces cerevisiae, a common yeast strain, was chosen in this work for a dual purpose. On one hand, it is an important model to exemplify the capabilities of such a microfluidic system and its direct applicability to the yeast fermentation industry (e.g. brewing,⁷ wine making,³³ baking,² biofuels,³⁴ and pharmaceutical protein production.³⁵ Through minor adjustments such a microfluidic system can also be used with mammalian,³⁶ insect,³⁷ and plant cells,³⁸ equally used in large-scale bioreactors.

System

The developed microfluidic platform and the method for assembling the components proved to be user-friendly, robust, reversible and leak free. The two types of microfluidic interconnections were self-aligned and easy to assemble, enabling the microfluidic chip to be replaced, without having to adjust the interconnections. Moreover, the developed connection method enabled tubings to be replaced individually. This added functionality prevents the need to fabricate new interconnections, or entire PDMS microfluidic ribbons as in earlier designs.^{26,39} An increase in performance was also observed as the used tubing does not wears off; thereby increasing the system lifetime, when compared with PDMS microfluidic ribbons. This is of extreme importance if one compares the micropumps RPM (120 RPM) used in the current system with the RPM used for cell culturing (0.1 RPM).³⁹ The modular nature of the used connections also ensures that the components can be easily arranged in a different configuration without having to fabricate new components.

For long term use of the platform, it is essential that the flow rate is stable in order to ensure the accuracy of the dilution factor and thereby correct determination of the cell concentrations. It is expected that the pump performance will be affected by components wearing off. The component most

likely to degrade is the tubing pressed between the roller pins and the rotor bed. According to the performed durability test, the micropump proved to have a stable flow rate with a low relative STD (3.8 %) for 243,000 rotations. Considering for instance the script S88, the number of pump rotations is calculated to be 236 and 39, corresponding to the pump drawing cell samples and the pump operating the diluent, respectively. Assuming that the fermentation process monitoring is performed once per hour, then the stable performance measured over 243,000 rotations, equal more than 1000 measurements and 42.9 days of consecutive operation exceeding the typical incubation times in bioreactors. The valve durability test was compared to the number of times the valves are actuated in script S88 (max. 15 times). Therefore, the 50,000 rotations measured when evaluating the valve performance correspond to performing 3333 measurements, which equal 138.9 days of operation. Furthermore, the valve compares positively with a previous design,²⁶ where the valve was only actuated for 20,000 rotations. Microfluidic devices containing integrated valves are typically based on the deflection of elastomeric membranes,^{24,25,40} however these components have rather limited lifetimes, due to the nature of the membrane material, and require external bulky actuators.⁴⁰ In the current system external valving was preferred in order to decrease the fabrication complexity of the microfluidic chip, as well as to further exploit the actuation mechanism developed for the micropumps. It is our observation that this approach proved to be the most adequate for this application, as the valve performance surpassed the initial requirements.

Adapting the manual dilution and staining protocols used in state of the art devices^{8,9} to a microfluidic system raised a whole new number of issues.

Air bubbles present in the ferment proved to be a major issue, as these tended to get trapped in the microfluidic device, more particularly in the slope leading to the imaging chamber, thus significantly influencing the measured cell concentration. When dealing with microfluidics, samples are often degassed by e.g. sonication before they are injected into the microfluidic channels. This is, however, not a valid option in the current system, few are the cases where administering of bubbles is implemented.⁴¹ Earlier implementations of the microfluidic chip only consisted of one outlet channel, which required that all the solutions had to pass through the imaging chamber, leading to unnecessary chamber contamination and more importantly to bubbles trapped in the slope merging the 0.5 mm deep channel to the 0.1 mm deep imaging chamber. This has been addressed by the introduction of an additional outlet channel (Figure 5 l) that prevents the imaging chamber from getting dirty with debris and cells. It furthermore allows removal of bubbles from the microfluidic chip before they enter the imaging chamber, due to the lower fluidic resistance in the secondary outlet channel (Figure 5 l). The implementation of intelligent procedures that take advantage of the robustness of the system enabled sufficient overpressures to be generated in the microfluidic chip, leading the air bubbles to collapse and to be subsequently flushed out, without any observed leaks.

Microfluidic devices implementing different mixing mechanisms have been extensively reported.^{11,42,43} However, these do not address mixing and dilution of cells in a wide dilution range as reported here. Cells due to their low diffusion coefficients are less prone to mix in comparison for e.g. fluorescent dyes, thus purely diffusive mixing is not applicable. Combining carefully designed curved microchannels and high flow rate operation enables cells to become well dispersed in

1 the meandering channel, due to the generation of Dean vortices.
2 The symmetric serpentine channel was successfully
3 implemented in order to promote the homogenization of the cell
4 distribution in the channel cross section, which otherwise
5 would be laminated. The symmetry of the serpentine channel
6 leads to a reversal of the transverse flow direction, which has
7 motivated the development of spiral structures for enhanced
8 mixing.²⁹ However, as the cells become already well distributed
9 in the first two to three turns of the serpentine channel, due to
10 the high rotation the fluid is subjected to, the fluid becomes
11 fully mixed in the remainder twenty four curves, before filling
12 the imaging chamber. The serpentine channel serves a dual
13 purpose as it is used for mixing the cell and fluorescent dye, but
14 it is equally used as a reservoir, so that five plugs can be
15 imaged in the 2.5 μl detection chamber, thus increasing the
16 statistical significance of the measured data. Curved planar
17 structures have the advantage of ease of fabrication, in
18 comparison to split and recombine structures and 3D serpentine
19 structures.^{44,45}

19 The calculated dilution factors are based on the addition of
20 merging flow rates, thus the theoretical error bar for each
21 dilution factor can be determined using the measured flow rates
22 and their standard deviation. For the three dilution factors an
23 error for the measured cell concentration of up to 6 % is
24 expected, where the possible error associated with the image
25 analysis method is not taken into account. This error is
26 calculated based on the larger relative STD observed at 5.5
27 $\mu\text{l}/\text{min}$ (5.3 %). The error on the flow rates, may in reality be
28 smaller, since possible errors from the flow sensor are not
29 considered. If a more realistic relative STD of 3 % is assumed,
30 as observed for the other measured flow rates, then the dilution
31 factors are expected to vary between 3.8 and 4.0 % for the 10,
32 88 and 259 times dilution. The larger relative STD observed in
33 Figure 8 is influenced by the dilution error, and also by the
34 image analysis error, which in this case consists of brightfield
35 imaging (< 5 %). The larger relative STD observed for S10 is
36 likely due to the high concentration of cells in the imaging
37 chamber, which considerably compromise the image analysis,
38 with respect to proper distinction of individual cells from cell
39 clusters. The manual control measurements were performed by
40 diluting 50 μl of cell sample in 450 μl of buffer solution. From
41 the experience acquired in our laboratory, dilution errors
42 between 5 and 10 % are customary for the used dilution factors,
43 especially when working with solutions at different
44 temperatures. Thus, the relative STDs obtained for the 10, 88
45 and 259 times are within the same range as for manual
46 dilutions.

47 The performance of the image analysis method proved to be
48 adequate, despite the 5 % deviation when determining the total
49 cell concentration using brightfield images. In fact, such a
50 deviation is nearly negligible (< 2 %) when calculating the
51 viability of cell samples, with viabilities larger than 70 %,
52 which most often is the case in the lag, exponentially and early
53 stationary growth phases. A possible method for improving the
54 image analysis in brightfield would be to use a higher
55 magnification, instead of the used 5x objective. The current
56 magnification enables 0.8 μl to be analyzed in one single
57 image, which corresponds to 1/3 of the imaging chamber
58 volume (2.5 μl). The use of a higher magnification would only
59 enable a very small volume to be analyzed per image, which
60 would then require the use of an automated stage scan, in order
to scan several areas within the chamber and in that way obtain
significant statistical data, or the analysis of several fluid plugs.
Alternatively, the image analysis could be made more robust by

avoiding bright field imaging. This could be achieved by
differential staining of the cell population using a cell-
impermeant dye (e.g propidium iodide) in combination with a
cell-permeant dye (e.g. Acridine Orange or Hoechst-33342).
Performing the tasks of collecting a cell sample, diluting the
plug, staining the cells and image acquisition has a total
duration of 10.3 min (Table 1 - s_1 , s_2 , $s_{3,ji}$ and s_2), which
surpasses the requirement of performing a control measurement
once per hour. Such a throughput is comparable with the
current commercial systems, where the dilution and staining
steps are performed manually,^{8,9} and furthermore eliminates
human-error from the analysis.

Conclusions

We have developed a fully automated microfluidic platform for
direct sampling from a bioreactor with a re-usable microfluidic
device. It handles the operations of 10 to 259 times sample
dilution, cell staining, image acquisition and image analysis,
with an analysis time of 10.3 min. The performance of the
platform was demonstrated by real-time monitoring of the
concentration and viability of yeast growing in a bioreactor
with a concentration of 10^5 to 10^8 cells/ml without any user
input. Furthermore, the performance of the multi-channel
peristaltic pumps and valves was characterized in terms of
reproducibility and robustness. They proved to have an
accuracy comparable to commercial pipettes during long time
use. This enabled exploiting Dean vortices for mixing and
homogenization of diluted cell samples, as well as the
implementation of automated protocols for administering air
bubbles trapped in the microfluidic chip.

The fluidic interconnections developed enabled self-alignment,
reversibility and easily assembled connections. The fluidic
components, such as pumps, valves, interconnections, etc. were
developed using a modular approach, which enables its use for
a multitude of applications where accurate fluidic control and
routing is highly important. The PMMA substrates chosen for
the fabrication of the microfluidic device proved to be an ideal
material in terms of optical transparency, low autofluorescence,
ease of fabrication, as well as high quality optical imaging for
both the brightfield and fluorescence image cytometry-based
detection. Furthermore, the platform and its components were
developed with the aim of being combined with existing
automated image analysis platforms, thus becoming a compact
and portable fully integrated system and avoiding the use of a
bulky microscope.

The ability to automate cell dilution, staining and image
analysis opens a wide repertoire of assays for improving
feedback controls used in bioreactors. Besides viability, other
physiological and metabolic parameters, such as apoptosis,
hypoxia and other stress related conditions can be quantified
and used to enhance the efficiency of bioreactors⁴⁶. Monitoring
additional parameters using the current developed platform can
be easily performed by adding adequate fluorescence markers
to the dilution buffer and recording the fluorescence signal in
different wavelength bands. Due to the adaptability of the
system, as well as the possibility to accurately tune flow rates
and sample dilutions, it is our belief that it can also be used
for monitoring the fermentation of mammalian, insect and plant
cells. Less robust cell lines than yeast, as is the case of
mammalian cells, are more susceptible to shear forces. Thus,
the impact of the high shear forces generated when diluting the
cell sample will be evaluated in future work in order to validate
the system versatility. Furthermore, as bioreactors working with

mammalian cells (up to 2×10^8 cells/ml) do not achieve as high concentrations as in the case of yeast or bacteria⁴⁷, we believe that dilution factors lower than 259 x will suffice, thus leading to smaller shear forces.

Acknowledgements

This work was supported by the Innovation Fund Denmark, grant 131-2013-5.

The authors would also like to acknowledge Johan Holm (ChemoMetec A/S) for the autofluorescence measurements demonstrating the suitability of PMMA as an imaging substrate.

Notes and references

^a Technical University of Denmark, Department for micro- and nanotechnology, Denmark. E-mail: paro@nanotech.dtu.dk

^b ChemoMetec A/S, Denmark.

Electronic Supplementary Information (ESI) available: The supplementary data document presents additional details regarding: S1 – Chip design and flow simulations, S2 – Experimental setup and S3 – Automated image analysis.

See DOI: 10.1039/b000000x/

References

- 1 N. Szita, P. Boccazzi, Z. Zhang, P. Boyle, A. J. Sinskey and K. F. Jensen, *Lab Chip*, 2005, **5**, 819–826.
- 2 D. Deere, J. Shen, G. Vesey, P. Bell, P. Bissinger and D. Veal, *Yeast*, 1998, **14**, 147–60.
- 3 L. L. Chan, E. J. Lyettefi, A. Pirani, T. Smith, J. Qiu and B. Lin, *J. Ind. Microbiol. Biotechnol.*, 2011, **38**, 1109–15.
- 4 J. Pattasseril, H. Varadaraju, L. Lock and J. a. Rowley, *Bioprocess Int.*, 2013, **11**, 46–52.
- 5 R. S. Martin, P. D. Root and D. M. Spence, *Analyst*, 2006, **131**, 1197–1206.
- 6 A. Lenshof and T. Laurell, *Chem. Soc. Rev.*, 2010, **39**, 1203–1217.
- 7 J. Novak, G. Basarova, J. a Teixeira, a a Vicente and J. I. Brew, *J. Inst. Brew.*, 2007, **113**, 249–255.
- 8 Nexcelom, <http://www.nexcelom.com/Applications/Yeast-Viability.html#feature2b>, 2014.
- 9 ChemoMetec, <http://chemometec.com/wp-content/uploads/2013/11/994-3031-Yeast-Viability-and-Count-using-the-PI-Cassette.pdf>, 2014.
- 10 P. van Hoek, E. de Hulster, J. P. van Dijken and J. T. Pronk, *Biotechnol. Bioeng.*, 2000, **68**, 517–23.
- 11 C.-Y. Lee, C.-L. Chang, Y.-N. Wang and L.-M. Fu, *Int. J. Mol. Sci.*, 2011, **12**, 3263–87.
- 12 D. J. Kim, H. J. Oh, T. H. Park, J. B. Choo and S. H. Lee, *Analyst*, 2005, **130**, 293–298.
- 13 Y. Li, F. Xu, C. Liu, Y. Xu, X. Feng and B.-F. Liu, *Analyst*, 2013, **138**, 4475–82.
- 14 S. L. Biswal and A. P. Gast, *Anal. Chem.*, 2004, **76**, 6448–55.
- 15 K.-R. Huang, Z.-H. Hong and J.-S. Chang, *Eur. J. Mech. - B/Fluids*, 2014, **48**, 153–164.
- 16 S. O. Catarino, L. R. Silva, P. M. Mendes, J. M. Miranda, S. Lanceros-Mendez and G. Minas, *Sensors Actuators B Chem.*, 2014, **205**, 206–214.
- 17 M. Jarrahi, C. Castelain and H. Peerhossaini, *Chem. Eng. Process. Process Intensif.*, 2013, **74**, 1–13.
- 18 A. P. Sudarsan and V. M. Ugaz, *Proc. Natl. Acad. Sci. U. S. A.*, 2006, **103**, 7228–7233.
- 19 S. Ahrar, M. Hwang, P. N. Duncan and E. E. Hui, *Analyst*, 2014, **139**, 187–90.
- 20 C. Kim, K. Lee, J. H. Kim, K. S. Shin, K.-J. Lee, T. S. Kim and J. Y. Kang, *Lab Chip*, 2008, **8**, 473–9.
- 21 J. Zhang, W. Li, M. Li, G. Alici and N.-T. Nguyen, *Microfluid. Nanofluidics*, 2013, **17**, 305–316.
- 22 Y. Abbas, J. Miwa, R. Zengerle and F. von Stetten, *Micromachines*, 2013, **4**, 80–89.
- 23 J. W. Hong, V. Studer, G. Hang, W. F. Anderson and S. R. Quake, *Nat. Biotechnol.*, 2004, **22**, 435–9.
- 24 F. Benito-Lopez, M. Antoñana-Díez, V. F. Curto, D. Diamond and V. Castro-López, *Lab Chip*, 2014, **14**, 3530–8.
- 25 I. E. Araci and S. R. Quake, *Lab Chip*, 2012, **12**, 2803–6.
- 26 D. Sabourin, P. Skafté-Pedersen, M. J. Sjøe, M. Hemmingsen, M. Alberti, V. Coman, J. Petersen, J. Emnéus, J. P. Kutter, D. Snakenborg, F. Jørgensen, C. Clausen, K. Holmstrøm and M. Dufva, *J. Lab. Autom.*, 2013, **18**, 212–28.
- 27 P. Skafté-Pedersen, D. Sabourin, M. Dufva and D. Snakenborg, *Lab Chip*, 2009, **9**, 3003–6.
- 28 G. M. Whitesides, *Lab Chip*, 2011, **11**, 191–3.
- 29 A. P. Sudarsan and V. M. Ugaz, *Lab Chip*, 2006, **6**, 74–82.
- 30 S. Ookawara, R. Higashi, D. Street and K. Ogawa, *Chem. Eng. J.*, 2004, **101**, 171–178.
- 31 A. Alrifaiy, O. a. Lindahl and K. Ramser, *Polymers (Basel)*, 2012, **4**, 1349–1398.
- 32 D. Mark, S. Haeberle, G. Roth, F. von Stetten and R. Zengerle, *Chem. Soc. Rev.*, 2010, **39**, 1153–82.
- 33 M. Ciani, I. Mannazzu, P. Marinangeli, F. Clementi and A. Martini, *Analysis*, 2004, **85**, 159–164.
- 34 A. a Vertès, M. Inui and H. Yukawa, *J. Mol. Microbiol. Biotechnol.*, 2008, **15**, 16–30.
- 35 J. L. Martínez, L. Liu, D. Petranovic and J. Nielsen, *Curr. Opin. Biotechnol.*, 2012, **23**, 965–71.
- 36 F. M. Wurm, *Nat. Biotechnol.*, 2004, **22**, 1393–8.
- 37 a Contreras-Gómez, a Sánchez-Mirón, F. García-Camacho, E. Molina-Grima and Y. Chisti, *Biotechnol. Prog.*, 2013, **30**, 1–18.
- 38 T.-K. Huang and K. a McDonald, *Biotechnol. Adv.*, 2012, **30**, 398–409.
- 39 P. Skafté-Pedersen, M. Hemmingsen, D. Sabourin, F. S. Blaga, H. Bruus and M. Dufva, *Biomed. Microdevices*, 2012, **14**, 385–99.
- 40 I. E. Araci and P. Brisk, *Curr. Opin. Biotechnol.*, 2014, **25**, 60–8.
- 41 M. Reichen, F. S. Veraitch and N. Szita, *J. Lab. Autom.*, 2013, **18**, 519–29.
- 42 Y. K. Suh and S. Kang, *Micromachines*, 2010, **1**, 82–111.
- 43 G. S. Jeong, S. Chung, C.-B. Kim and S.-H. Lee, *Analyst*, 2010, **135**, 460–73.
- 44 D. S. Kim, S. H. Lee, T. H. Kwon and C. H. Ahn, *Lab Chip*, 2005, **5**, 739–47.
- 45 R. H. Liu, M. a. Stremmler, K. V. Sharp, M. G. Olsen, J. G. Santiago, R. J. Adrian, H. Aref and D. J. Beebe, *J. Microelectromechanical Syst.*, 2000, **9**, 190–197.

Analyst

- 1
2 46 L. L. Chan, A. Kury, A. Wilkinson, C. Berkes and A. Pirani, *J. Ind.*
3 *Microbiol. Biotechnol.*, 2012, **39**, 1615–23.
4 47 M. F. Clincke, C. Mölleryd, Y. Zhang, E. Lindskog, K. Walsh and V.
5 Chotteau, *Biotechnol. Prog.*, 2013, **29**, 754–767.
6
7
8
9
10
11
12
13
14
15
16
17
18
19
20
21
22
23
24
25
26
27
28
29
30
31
32
33
34
35
36
37
38
39
40
41
42
43
44
45
46
47
48
49
50
51
52
53
54
55
56
57
58
59
60